STM JOURNALS

Journal of
Polymer & Composites

ISSN: 2321-2810 (Online)
ISSN: 2321-8525 (Print)
Volume 12, Special, Issue 6, 2024
DOI (Journal): 10.37591/JoPC

https://journals.stmjournals.com/jopc

Research JoPC

Synthesis and Characterization of Mn^{2+} Doped $LiPbX_3$(X = Cl, Br, I)

Aparna J. Nadgowda[1,*], Shashi B Pandey[1], Chitra S Khade[1], Purushotam K. Naktode[2]

Abstract

In this paper the structural, electronic and optical properties of Mn doped Pb based cubic perovskites $LiPbX_3$(X= Cl, Br and I) were studied by wet chemical method (sol gel method). For Mn doped $LiPbX_3$(X= Cl, Br and I) NCs, MnCl2 and $PbBr_2$ were added in molar feed ratio 1.35 mole% and nan crystal were examine with the help of TEM and their structure were confirmed by X-ray diffraction (XRD). Additionally, the Mn^{2+} ions in the $LiPb(Cl/Br)_3$ are responsible for the wide emission at 603 nm, which has been attributed to a transition between the $^4T_1$ and $^6A_1$ energy level of Mn^{2+} 3d states. This emission characteristic indicates the potential of these Mn-doped perovskites for applications in optoelectronic devices, such as light-emitting diodes (LEDs) and phosphors. This study highlights the importance of dopant incorporation in tuning the electronic and optical properties of perovskite materials, paving the way for further exploration and development in the field of nanomaterials and optoelectronics. This paper investigates the structural, electronic, and optical properties of Mn-doped Pb-based cubic perovskites $LiPbX_3$ (X= Cl, Br, and I) synthesized using the sol-gel method. TEM and XRD were employed to confirm the nanocrystals' structure, while the Mn^{2+} ions in $LiPb(Cl/Br)_3$ were found to emit at 603 nm, due to transitions between the $4T_1$ and $6A_1$ energy levels of Mn^{2+} 3d states.

Keywords: Perovskites, luminescent properties, lighting application, nanomaterial, optoelectronic applications

INTRODUCTION

In recent research community perovskites materials attract special attention due to their special characteristics such as electronic properties, photo luminescent properties, and physical properties as they are widely used in solar cell or other optoelectronic devices [1]. In today's era the pervoskites materials had become the most interesting research area worldwide due to fascinating optoelectronic properties, various uses, and simplistic synthesis techniques. It has been confirmed that the pervoskites materials are widly used in solar cell due to their superb efficiency. But mass production of perovskite solar cells (PSCs) for commercialization is still a ways off due to their modest stability [2, 3]. The three materials are all semiconductors by nature, according to their electrical characteristics. For LiPbCl3, LiPbBr3, and LiPbI3, the estimated energy band gaps are 1.801 eV, 2.337 eV, and 1.943 eV, respectively. To describe the interaction of light with the material, the optical characteristics of all three materials are discussed for photon energies that vary from 0 to 25 eV [4-6]. The identification of perovskite materials with superior optoelectronic properties derived from low-toxicity elements like Sn, Bi, Sb, Ge, and Cu offers substitute methods for achieving high-performance perovskite optoelectronics. The broad colour gamut, high chromatic purity, ultrahigh visual resolution, and small pixel size of advanced display devices make

***Author for Correspondence**
Aparna J. Nadgowda
E-mail: aparna.pimple@raisoni.net

[1]Research Scholar, Department of Physics, G.H. Raisoni University, Amravati, Maharashtra, India
[2]Assistant Professor, Department of Physics, G.H. Raisoni Institute of Engineering and Technology, Nagpur, Maharashtra, India

Received Date: May 14, 2024
Accepted Date: July 19, 2024
Published Date: August 08, 2024

Citation: Aparna J. Nadgowda, Shashi B Pandey, Chitra S Khade, Purushotam K. Naktode. Synthesis and Characterization of Mn^{2+} Doped $LiPbX_3$(X = Cl, Br, I). Journal of Polymer & Composites. 2024; 12(6): S48–S54p.

them more in demand. As functional films, light sources, backlight components, and display panels, all-inorganic lead halide perovskite (AILHP) nanocrystals (NCs) have been created because of their inherent benefits, which include narrow emission width, saturated colour, and flexible integration [7]. There are several generations of solar cells in the photovoltaic business, each with unique benefits and difficulties. High power conversion efficiency (PCE) and stability are provided by first-generation cells based on monocrystalline and polycrystalline silicon wafers; the disadvantage is their high production cost. Thin-film-based second-generation cells, such as CdTe and CIGS, provide lower manufacturing costs, flexible substrates, and a wider range of potential applications; nevertheless, their efficiency and stability are often lower. Emerging and third-generation PV technologies, like quantum dot solar cells, PSCs, DSSCs, CZTS, and organic photovoltaics, are promising for greater PCEs with new applications but have stability and scalability issues [8].

Synthesis Process

Wet chemical synthesis methods are commonly used for the preparation of perovskite materials like LiPbX3 (where X = Cl, Br, I). Here, we follow a general procedure for the wet chemical synthesis of $LiPbX_3$ compounds using lithium halide (LiX) and lead halide (PbX_2) as starting materials. We weigh the appropriate amounts of lithium halide (LiX) and lead halide (PbX_2) according to the desired stoichiometric ratio. Ensure precision in measurements for accurate results. Then we dissolve lithium halide (LiX) in a suitable solvent (e.g., DMF, DMSO) to create a lithium halide solution. Stir the solution until the LiX is completely dissolved. Similarly, dissolve lead halide (PbX_2) in the same or a separate container using the same solvent to create a lead halide solution. We was stir this solution until the PbX_2 is fully dissolved. Then we combine the lithium halide solution and the lead halide solution in the desired stoichiometric ratio (1:1 for $LiPbX_3$) in a reaction vessel (e.g., flask or beaker). Stir the mixture thoroughly to ensure homogeneity [9].

As we mix the solutions, a white or yellow precipitate of $LiPbX_3$ start to form. This is the desired perovskite product. Once the precipitation is complete, we separate the solid $LiPbX_3$ product from the solution using vacuum filtration or gravity filtration with filter paper [10]. We wash the collected solid product with a suitable solvent (e.g., ethanol or acetone) to remove impurities and any unreacted starting materials. Wash until the filtrate is clear.

Transfer the washed $LiPbX_3$ precipitate to a clean container and allow it to air dry or place it in an oven at a low temperature (e.g., 50-80°C) to ensure complete drying. This step is essential to remove any remaining solvent. To verify the structural composition & purity synthesized $LiPbX_3$ sample we use XRD, FTIR & SEM analysis as a characterisation techniques [11, 12].

RESULTS AND DISCUSSION

To make the Mn-doped $LiPb(Cl/Br)_3$ NCs, $MnCl_2$ is added to $PbBr_2$ precursors in a colloidal solution. The water is evaporated from a combination of OA, OAm, and ODE at 120°C while the molar feed ratio of MnCl2 and PbBr2 is 1.35. After that, it's crucial to heat everything up over 200° degrees Celsius to fully dissolve the metal salts. The temperature is decreased to 180° to synthesis $LiPb(Cl/Br)_3$ nanocrystals doped with Mn^{2+}. Nanostructures of Mn-doped $LiPb(Cl/Br)_3$ NCs were obtained by transmission electron microscopy (TEM) after their preparation. TEM analysis of as-prepared Mn-doped $LiPb(Cl/Br)_3$ NCs reveals that they are cubic in shape and average 11.5 nm in size. The Mn-doped $LiPb(Cl/Br)_3$ NCs' phase structure was determined with the help of X-ray diffraction (XRD). In comparison to undoped cubic $LiPbCl_3$ nanocrystals (space group Pm3m, PDF#73-0692), all of the diffraction peaks of Mn-doped $LiPb(Cl/Br)_3$ NCs shifted slightly to lower angles. This may be because the cell size increases after Br ion incorporation into LiPbCl3 NCs, causing all the peaks to shift to lower angles. In addition, the XRD results demonstrate that the as-prepared Mn doped $LiPb(Cl/Br)_3$ NCs may be assigned to the same cubic phase as the undoped $LiPbCl_3$ NCs, suggesting that the rigidity of the cationic framework of the perovskite prevents any changes to the crystal structure during the doping process [13, 14]. According to a high-resolution transmission electron microscopy (HRTEM) picture shown in Figure 1, the interplanar spacing of its (100) plane set is 5.69 A^0, which is bigger than

the 5.6˚ A˚ of $LiPbCl_3$. This also shows that the Mn doped NC in its as-prepared form has $LiPb(Cl/Br)_3$ as its host. High crystalline nature of Mn doped $LiPb(Cl/Br)_3$ NCs is reflected by broad XRD peaks and a HRTEM picture.

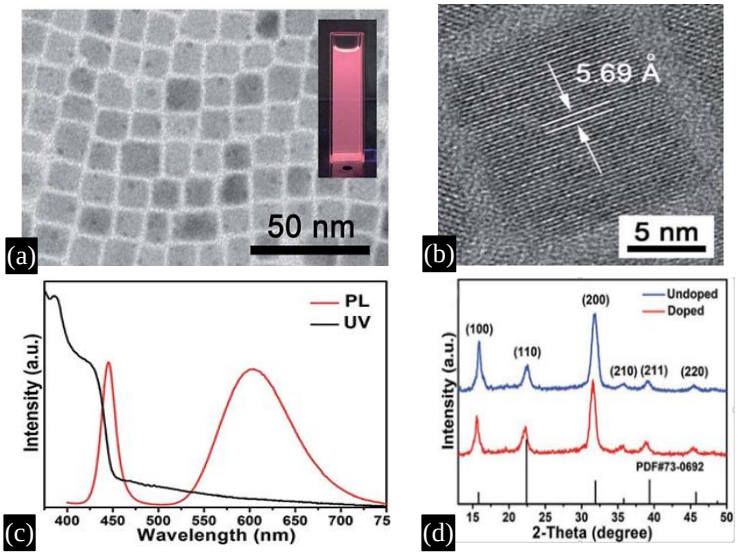

Figure 1. TEM image (a), HRTEM image (b), PL emission and UV-vis absorption spectra (c) and XRD pattern of Mn-doped $LiPb(Cl/Br)_3$ NCs (d). Inset in (a): PL image excited by 365 nm UV light.

Measuring the UV-vis absorption and photoluminescence spectra of Mn-doped $LiPb(Cl/Br)_3$ NCs dispersed in cyclohexane allowed us to learn more about their optical characteristics after synthesis. Under a 365 nm UV-lamp, the Mn-doped $LiPb(Cl/ Br)_3$ NCs solution emits a deep pink hue. At 424 nm, the Mn-doped $LiPb(Cl/Br)_3$ NCs exhibit a strong absorption peak. Dual-color emissions are clearly visible in the PL spectrum. The $LiPb(Cl/Br)_3$ host is credited with the narrow band emission centred at 445 nm and having a full width at half maximum of 18 nm. Additionally, the Mn^{2+} ions doped in the $LiPb(Cl/Br)_3$ NCs are responsible for the wide emission at 603 nm with a full width at half maximum (FWHM) of 87.5 nm, which has been attributed to a transition between the $^4T_1$ and $^6A_1$ energy levels of the Mn^{2+} 3d states. In Figure 2, we can see the energy levels and fluorescence mechanism of Mn-doped $LiPb(Cl/Br)_3$ NCs [15, 16].

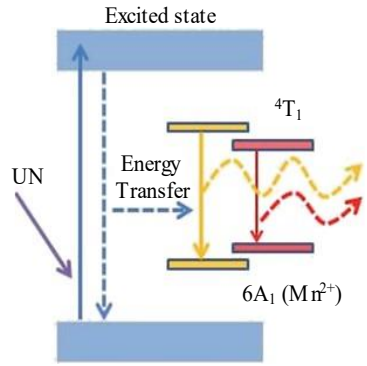

Figure 2. Energy levels and fluorescent mechanism of Mn-doped $LiPb(Cl/Br)_3$ NCs<>.

The strong fluorescence of Mn^{2+} ions demonstrates that the doped Mn^{2+} ions might be used as an effective acceptor of the energy from the excited $LiPb(Cl/Br)_3$ host as shown in Figure 2. However, the PL spectrum provides adequate confirmation of the presence of Mn^{2+} ions in the as-prepared $LiPb(Cl/Br)_3$ NCs, despite the lack of microscopical evidence that these ions are integrated into the lattice.

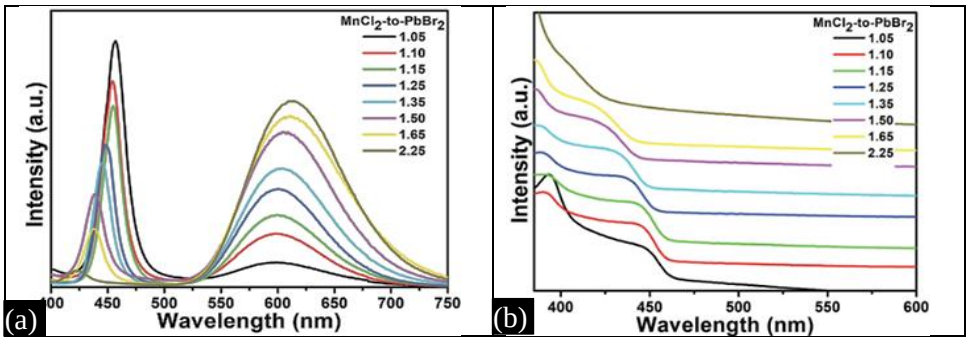

Figure 3. PL emission spectra (a) and absorption spectra (b) of the Mn-doped $LiPb(Cl/Br)_3$ NCs prepared with different $MnCl_2$-to-$PbBr_2$ molar feed ratio at 180°C.

Modifying the $MnCl_2$-to-$PbBr_2$ molar feed proportion results in Mn-doped $LiPb(Cl/Br)_3$ NCs with tunable optical characteristics. At a constant 180°C, Figure 3 (a) displays the photoluminescence (PL) spectra of Mn-doped $LiPb(Cl/Br)_3$ NCs prepared using a range of $MnCl_2$-to-$PbBr_2$ molar feed ratios (1.05 to 2.25). As was previously indicated, the Mn-doped $LiPb(Cl/Br)_3$ NCs emit both $LiPb(Cl/Br)_3$ host and Mn^{2+} ions. As the cl to Br molarfeed ratio increased, the photoluminescence wavelength decreased from 457nm to 422 nm. The UV-vis absorption curve shifts slightly toward the blue as the Br/Cl molar ratio is altered. Concurrently, a red shift is visible from 597 nm to 613 nm in the Mn^{2+} ions' wide emission. Because the energy gap of $^4T_1$-$^6A_1$ narrowed as Mn % increased, the emitted Mn^{2+} ions shifted to the red. The Mn^{2+} substitution ratio in the $LiPb(Cl/Br)_3$ host is low because the molar feed ratio of $MnCl_2$ to $PbBr_2$ is small. To put it another way, the $LiPb(Cl/Br)_3$ host would interfere with the energy transfer of the Mn^{2+} ions, preventing them from emitting. However, the exciton-to- Mn^{2+} energy transfer may be improved by raising the $MnCl_2$-to-$PbBr_2$ molar feed ratio, which enhances the Mn^{2+} substitution ratio in the $LiPb(Cl/Br)_3$ host. We used inductively coupled plasma to find the elemental distribution (ICP). The Mn^{2+}substitution ratio grows from 1.50% to 2.33% when the $MnCl_2/PbBr_2$ molar feed ratio grows from 1.05 to 2.25. In this way, the emission of Mn^{2+} ions is substantially amplified while the emission of the $LiPb(Cl/Br)_3$ host progressively fades, leading to an increase in the orange emission. Also, the PLQYs of the Mndoped $LiPb(Cl/Br)_3$ NCs generated with a 1.05 to 1.65 molar feed ratio of $MnCl_2$- to-$PbBr_2$ go up from 14.3 to 38.2% as the PL intensity of Mn^{2+} ions rises. Due in large part to a drop in host PLQY, the produced NCs show a modest slowing in PLQY, down to 37.1%, when the $MnCl_2$-to-$PbBr_2$ molar feed ratio is 2.25.

Table 1 compiles the PLQYs of Mn-doped $LiPb(Cl/Br)_3$ NCs produced with varying molar input ratios of $MnCl_2$ to $PbBr_2$. These findings demonstrate that the optical characteristics of Mn-doped $LiPb(Cl/Br)_3$ NCs may be finely tuned by adjusting the $MnCl_2/PbBr_2$ molar feed proportion in the precursor solution.

Table 1. The PLQYs of the Mn-doped CsPb(Cl/Br)3 NCs prepared with different MnCl2-to-PbBr2 molar feed ratio and reaction temperature

S.N.	MnCl2-to-PbBr2 molar feed ratio	Reaction temperature °C)	PLQY (%)
1	1.05	180	14.3
2	1.10	180	15.6
3	1.15	180	16.8
4	1.25	180	22.1
5	1.35	180	25.7
6	1.50	180	34.6
7	1.65	180	38.2
8	2.25	180	37.1
9	1.35	160	15.0
	1.35	200	33.9

X-ray diffraction (XRD) patterns of Mn-doped LiPb(Cl/Br)$_3$ NCs at various MnCl2-to-PbBr2 molar feed ratios are displayed in Figure 4 (from 1.05 to 2.25). From XRD (PDF#73-0692) we can say that the molar feed ration of Cl to Br have no effect on their structure, they all have same crystalline cubic structure. Increasing the molar feed ratio of $MnCl_2$ to $PbBr_2$ also causes all of the diffraction peaks in the XRD patterns to move to larger angles. For the simple reason that when Cl ions combine, the cell shrinks and all the peaks shift to greater angles. These findings are consistent with those reported previously for anion exchange processes that make use of Pb-based halide precursors or oleylammonium halide precursors.

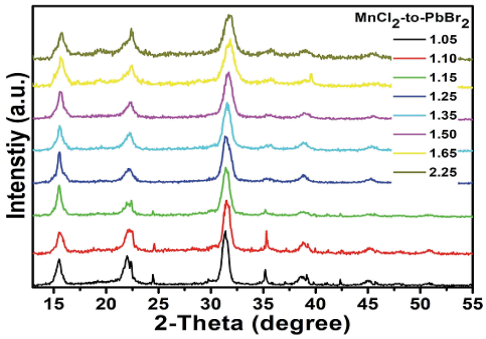

Figure 4. XRD patterns of the Mn-doped LiPb(Cl/Br)$_3$ NCs with different $MnCl_2$-to-$PbBr_2$ molar feed ratio

The Mn-doped LiPb (Cl/Br)3 NCs were produced, and their nanostructures were obtained using TEM. samples produced with different molar input ratios of $MnCl_2$ to $PbBr_2$ share a similar cubic shape and modest size fluctuation, as seen in TEM images. As the MnCl2-to-PbBr2 molar input ratio is raised from 1.05 to 2.25, the size of the as-prepared Mn-doped LiPb(Cl/Br)3 NCs gradually decreases. The related particle size distribution and PL pictures of the nanocrystal cyclohexane solution stimulated by 365 nm UV light can be seen in the insets of the TEM photos.

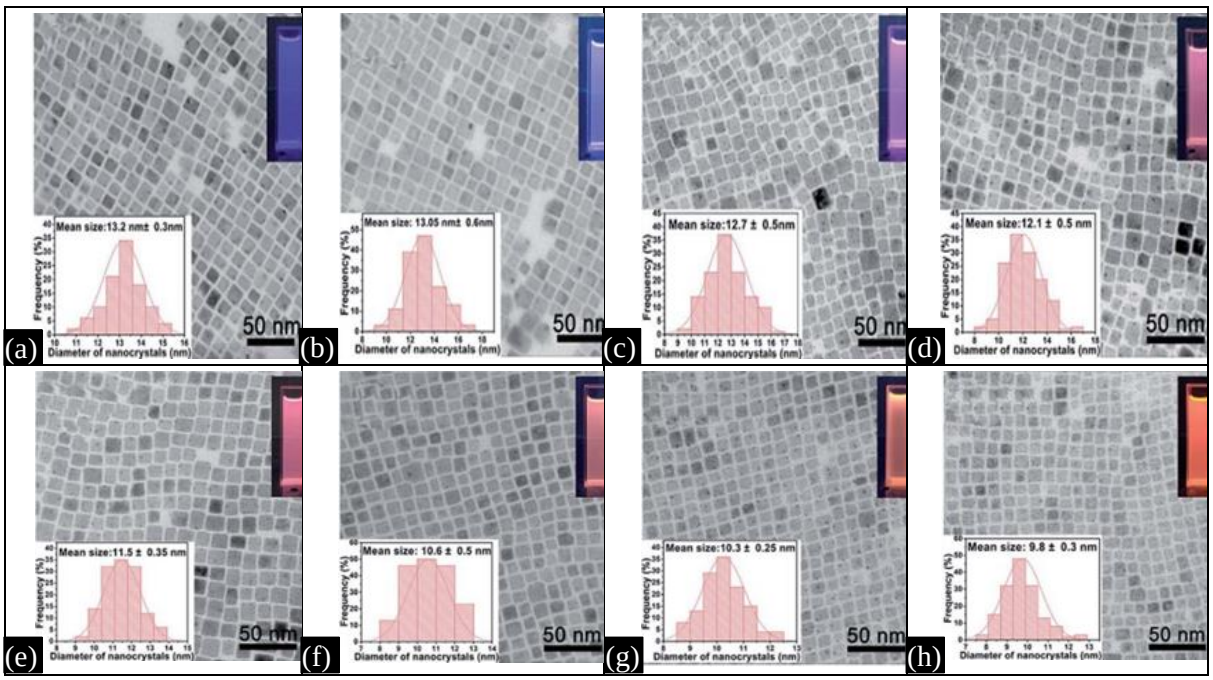

Figure 5. Transmission electron microscope (TEM) images of the Mn-doped LiPb(Cl/Br)$_3$ NCs with different $MnCl_2$-to-$PbBr_2$ molar feed ratio: (a) 1.05, (b) 1.10, (c) 1.15, (d) 1.25, (e) 1.35, (f) 1.50, (g) 1.65, (h) 2.25. Insets: corresponding particle size distribution and PL images excited by 365 nm UV light.

The CIE (Commission Internationale de I'Eclairage 1931 chromaticity) chromaticity coordinates were derived and displayed to assess the performance of Mn-doped $LiPb(Cl/Br)_3$ NCs on colour luminescent emission with varying $MnCl_2$-to-$PbBr_2$ molar feed ratio. The matching PL pictures of the nanocrystal cyclohexane solution triggered by 365 nm UV light show that the colour hue of the Mn-doped $LiPb(Cl/Br)_3$ NCs can be controlled accurately, as shown in the graph presented in Figure 6.

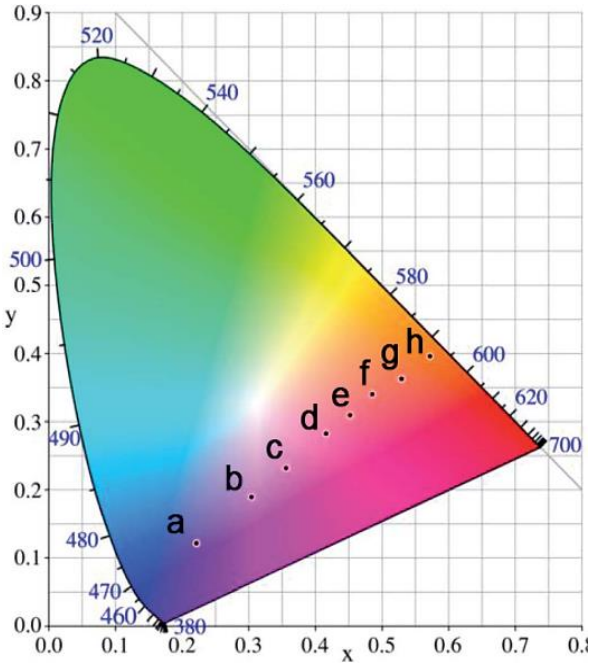

Figure 6. CIE chromaticity diagram of the Mn-doped LiPb(Cl/Br)3 NCs prepared with different $MnCl_2$-to-$PbBr_2$ molar feed ratio: (a) 1.05, (b) 1.10, (c) 1.15, (d) 1.25, (e) 1.35, (f) 1.50, (g) 1.65, (h) 2.25.

Doping Mn^{2+} ions into $LiPb(Cl/Br)_3$ NCs is a thermodynamically regulated procedure, just like doping Mn^{2+} ions into CdSe or ZnSe NCs. The PL spectrum of Mn-doped $LiPb(Cl/Br)_3$ NCs at several reaction temperatures is shown in Figure 5, where the molar feed ratio of $MnCl_2$ to $PbBr_2$ was held constant.

CONCLUSION

In summary, we reported the successive and accurate adjustment of Photoluminescence emission peak of Mn doped $LiPbCl/Br)_3$ in the range from 597 nm to 613 nm caused red shift because energy gap of $^4T_1$- $^6A_1$ and narrow as Mn% increased. The finding demonstrate that the optical characteristics of Mn doped $LiPbCl/Br)_3$ Ncs may be finally tuned by adjusting the $MnCl_2$/ $PbBr_2$ molar feed ratio. The ability to control photoluminescence emission intensities throughout a broad colour spectrum suggests that these materials have potential use in light-emitting devices.

REFERENCES

1. Elangovan NK, Kannadasan R, Beenarani BB, Alsharif MH, Kim MK, Inamul ZH. Recent developments in perovskite materials, fabrication techniques, band gap engineering, and the stability of perovskite solar cells. 2024;11:1171–1190.
2. Chilvery A, Palwai S, Guggilla P, Wren K, Edinburgh D. Perovskite Materials: Recent Advancements and Challenges. Submitted: 22 March 2019 Reviewed: 09 July 2019 Published: 05 September 2019.
3. Kojima A. Organometal Halide Perovskites as Visible-Light Sensitizers for Photovoltaic Cells. J Am Chem Soc. 2009 May;131(17):6050–1.
4. Li J, Duan J, Yang X, Duan Y, Yang P, Tang Q. Review on recent progress of lead-free halide perovskites in optoelectronic applications. 2021;80:105526.

5. Miaha MH, Khandaker MU, Rahman MB, Nur-E-Alamd M, Islam MA. Band gap tuning of perovskite solar cells for enhancing the efficiency and stability: issues and prospects. RSC Adv. 2024;14:15876–15906.
6. Rehman MA, ur Rehman J, Tahir MB. A DFT study of structural, electronic, optical, mechanical, thermoelectric, and magnetic properties of Pb-halide perovskites LiPbX3 (X = Cl, Br, and I) for photovoltaic applications. 2023;1223:114085.
7. Mohammed, Koh SCL, Reaney IM, Acquaye A, Schileo G, Mustapha KB, Greenough R. Perovskite solar cells: An integrated hybrid lifecycle assessment and review in comparison with other photovoltaic technologies. 2017;80:1321–1344.
8. Noman M, Khan Z, Jan ST. A comprehensive review on the advancements and challenges in perovskite solar cell technology. RSC Adv. 2024;14:5085–5131.
9. Huang YT, Kavanagh SR, Scanlon DO, Walsh A, Hoye RLZ. Perovskite-inspired materials for photovoltaics and beyond—from design to devices. Nanotechnology. 2021;32(13).
10. Zhu T, Yang Y, Gong X. Recent Advancements and Challenges for Low-Toxicity Perovskite Materials. ACS Appl Mater Interfaces. 2020;12(24):26776–26811.
11. Ikram M, Malik R, Raees R, Imran M, Wang F, Ali S, Khan M, Khan Q, Maqbool M. Recent advancements and future insight of lead-free non-toxic perovskite solar cells for sustainable and clean energy production: A review. 2022;53(Part A):102433.
12. Yang D, Cao M, Zhong Q, Li P, Zhang X, Zhang Q. All-inorganic cesium lead halide perovskite nanocrystals: synthesis, surface engineering and applications. J Mater Chem C. 2019;7(4).
13. Sun S. Mechanical Properties of Organic-Inorganic Halide Perovskites, CH3NH3PbX3 (X=I, Br and Cl) by Nanoindentation. 2015;3(36):18450–18455.
14. Kumar D, Yadav RS, Monika, Singh AK, Rai SB. Synthesis Techniques and Applications of Perovskite Materials. Submitted: 12 March 2019 Reviewed: 13 May 2019 Published: 10 June 2020.
15. Atta NF, Galal A, El-Ads EH. Perovskite Nanomaterials – Synthesis, Characterization, and Applications. Submitted: 31 March 2015 Reviewed: 18 August 2015 Published: 03 February 2016.
16. Wang P, Dong B, Cui Z, Gao R, Su G, Wang W, et al. Synthesis and characterization of Mn-doped CsPb(Cl/Br)3 perovskite nanocrystals with controllable dual-color emission. RSC Adv. 2018;8(4):1940–1947.

